Three-dimensional solar radiation effects on the actinic flux field in a biomass-burning plume

Jörg Trentmann[1,2], Barbara Früh,[3] Olivier Boucher,[1,4] Thomas Trautmann,[5,6] and Meinrat O. Andreae[1]

Received 16 January 2003; revised 16 May 2003; accepted 5 June 2003; published 12 September 2003.

[1] Three-dimensional (3-D) solar radiative transfer models describe radiative transfer under inhomogeneous atmospheric conditions more accurately than the commonly used one-dimensional (1-D) radiative transfer models that assume horizontal homogeneity of the atmosphere. Here results of 3-D radiative transfer simulations for a biomass-burning plume are presented and compared with local one-dimensional (l-1-D) simulations, i.e., 1-D simulations in every column of the model domain. The spatial distribution of the aerosol particles was derived from a 3-D atmospheric transport simulation. We studied the impact of 3-D radiative effects on the actinic flux within the plume center. The differences in the actinic flux between results from the 3-D and the l-1-D simulations are considerable, ranging from −40% to more than +200%, depending on the wavelength, solar zenith angle, and the absorbing properties of the aerosol. The reason for this discrepancy is the neglect of horizontal photon transport in the 1-D simulation. These large 3-D effects on the actinic flux have the potential to influence significantly the in-plume photochemistry. *INDEX TERMS:* 0305 Atmospheric Composition and Structure: Aerosols and particles (0345, 4801); 0345 Atmospheric Composition and Structure: Pollution—urban and regional (0305); 3359 Meteorology and Atmospheric Dynamics: Radiative processes; *KEYWORDS:* biomass burning plume, actinic flux, 3-D solar radiative transfer simulations, aerosol absorption

Citation: Trentmann, J., B. Früh, O. Boucher, T. Trautmann, and M. O. Andreae, Three-dimensional solar radiation effects on the actinic flux field in a biomass-burning plume, *J. Geophys. Res.*, *108*(D17), 4558, doi:10.1029/2003JD003422, 2003.

1. Introduction

[2] Radiative transfer in the atmosphere is a three-dimensional process. Nevertheless, commonly used radiative transfer models only consider vertical photon transfer and assume that the atmosphere is homogeneous in the horizontal directions. This assumption of one-dimensional (1-D) radiative transfer is a good approximation for clear-sky conditions over a uniform surface, but is generally not fulfilled if aerosol plumes or clouds are present or if the surface does not have uniform properties. A prominent example for an inhomogeneous aerosol distribution is a biomass-burning plume. Such a plume has comparable small spatial dimensions and high aerosol loadings, with aerosol optical depths (AOD) values of 3 in the visible spectrum downwind of the fire [e.g., *Ferrare et al.*, 1990; *Liousse et al.*, 1995; *Gassó and Hegg*, 1998]. AOD values immediately above the fire are expected to be even higher.

[3] In the past, three-dimensional distributions of cloud droplets and aerosol particles were often not available for atmospheric studies, since the resolution of global circulation models and satellite instruments was too coarse. High resolution in situ measurements are rare and can only yield very limited information about the spatial distribution of particles. Recently, significant improvements in the resolution of atmospheric models and remote sensing instruments were achieved. Large-eddy simulation (LES) models have become a valuable modeling tool [e.g., *Duynkerke et al.*, 1999; *Vilà-Guerau de Arellano and Cuijper*, 2000; *Stevens et al.*, 2001] along with convective cloud and plume models [e.g., *Oberhuber et al.*, 1998; *Lu et al.*, 2000; *Skamarock et al.*, 2000; *Khairoutdinov and Randall*, 2003]. Meanwhile, modern satellite and airborne remote sensing instruments are able to observe the atmosphere with a horizontal resolution at the order of one kilometer in case of spaceborne instruments (such as the Moderate Resolution Imaging Spectroradiometer (MODIS), the Medium Resolution Imaging Specrometer Instrument (MERIS), and the Cloud-Aerosol Lidar and Infrared Pathfinder Satellite Observations (CALIPSO)) and a few tens of meters in the case of airborne instruments (such as the MODIS airborne simulator (MAS) and the Airborne Visible Infrared Imaging Spectrometer (AVIRIS)). Thus the possibility and need of detailed studies

[1]Biogeochemistry Department, Max Planck Institute for Chemistry, Mainz, Germany.
[2]Now at Department of Atmospheric Sciences, University of Washington, Seattle, Washington, USA.
[3]Institute for Atmospheric Physics, University of Mainz, Mainz, Germany.
[4]Laboratoire d'Optique Atmosphérique, CNRS/USTL, UMR 8518, Villeneuve d'Ascq, France.
[5]Institute for Meteorology, University of Leipzig, Leipzig, Germany.
[6]Now at Institut für Methodik der Fernerkundung, Deutsches Zentrum für Luft- und Raumfahrt e.V. (DLR), Oberpfaffenhofen, Wessling, Germany.

0148-0227/03/2003JD003422$09.00

on the effects of horizontally inhomogeneously distributed particles on the atmospheric radiation field arise. For these investigations, three-dimensional (3-D) radiative transfer models have to be used.

[4] The modification of the reflected radiation field due to cloud inhomogeneities has drawn special attention, because of the nonlinearity between cloud optical depth and cloud albedo. The mean albedo of a cloud with horizontally varying optical depth is less than the albedo of a uniform cloud with the same mean optical depth. This effect is called the ''plane-parallel albedo bias'' (PPA) [*Cahalan et al.*, 1994]. This needs to be taken into account in global circulation models, which simulate only the averaged cloud optical depth within a grid box.

[5] Additionally, it was suggested that cloud inhomogeneities are at least in part responsible for the discrepancy between modeled and observed absorption within clouds [*Cess et al.*, 1995; *Ramanathan et al.*, 1995]. The effect of cloud inhomogeneities on atmospheric absorption is a complex interplay between gaseous absorption, cloud droplet absorption, and solar inclination. There have been studies on the effect of cloud inhomogeneities on atmospheric absorption, indicating that they are, at least in part, responsible for the enhanced absorption that is observed [*Borde and Isaka*, 1996; *O'Hirok and Gautier*, 1998a, 1998b; *Cairns et al.*, 2000].

[6] A similar underestimation of atmospheric absorption is observed when model results are compared with measurements in the cloud-free atmosphere in the presence of aerosol particles [*Kato et al.*, 1997; *Wild*, 1999; *Halthore and Schwartz*, 2000]. However, the possible effects of inhomogeneities in the spatial distribution of the aerosol on the atmospheric radiation field have not been addressed yet. So far, the spatial distribution of the aerosol is assumed to be horizontally homogeneous on the scale of some tens of kilometers, which would allow the independent pixel approximation (IPA) to be employed in radiative transfer simulations. Nevertheless, this assumption is not valid for an individual plume (or a set of individual plumes, e.g., from vegetation fires). Recently, *Lyapustin and Kaufman* [2001] used a 3-D radiative transfer model to investigate the role of the spatial heterogeneity of land surfaces on aerosol remote sensing. However, only horizontally homogeneous aerosol distributions were used in the simulations.

[7] Two different types of heterogeneity effects can be distinguished [*Várnai and Davis*, 1999; *Benner and Evans*, 2001]: the one-dimensional heterogeneity effect and the horizontal transport effect. The one-dimensional heterogeneity effect is caused by the nonlinearity between cloud optical depth and albedo (also called PPA, as mentioned before) [*Cahalan et al.*, 1994]. The horizontal transport effect results from the horizontal transfer of direct or scattered radiation between adjacent columns. Photons within a cloud or an aerosol plume can leak out through the sides due to scattering processes or enter the cloud or aerosol plume from the side due to direct illumination or scattering.

[8] The one-dimensional heterogeneity effect can be addressed with 1-D models based on the independent pixel approximation (IPA) [*Cahalan et al.*, 1994]. In the IPA, 1-D radiative transfer simulations are performed independently in every column of the model domain and the results of these simulations are horizontally averaged. Horizontal transport of photons between adjacent columns is not taken into account. A first attempt to improve the IPA is the tilted IPA (TIPA) that takes into account the horizontal transfer of the direct solar radiation by orienting the vertical columns along the slant path of the incoming solar photons [*Várnai and Davis*, 1999]. However, side leakage and radiative smoothing [*Marshak et al.*, 1995] can only be considered in 3-D radiative transfer simulations.

[9] While IPA is a good approximation for the averaged radiation field, high-resolution atmospheric models, e.g., cloud-resolving models or large eddy simulations (LES), require the calculation of the local radiation field in each grid cell of the model. This is especially true for chemistry models, which require the calculation of local photolysis frequencies. As those high-resolution atmospheric models are often designed to simulate clouds and/or plumes, large horizontal gradients are not uncommon. Nevertheless, the radiation transfer equation is usually solved for each model column independently, implicitely assuming horizontal homogeneity [e.g., *Xu and Randall*, 1995; *Lu et al.*, 2000; *Wang and Prinn*, 2000; *Trentmann et al.*, 2002; *Khairoutdinov and Randall*, 2003]. By doing so, horizontal gradients of the atmospheric composition, e.g., the cloud water, result in gradients in the radiation field. Horizontal averaging would result in unrealistic smoothing of the radiation field. In the following, we refer to the way the local radiation field in high-resolution atmospheric models is calculated as local one-dimensional radiative transfer simulations (l-1-D).

[10] Most previous studies of three-dimensional radiative effects focused on the reflected or transmitted irradiance. However, in high-resolution atmospheric models, the local actinic flux is of special importance, because the local heating rates and the photolysis frequencies are derived from this quantity. Potential three-dimensional solar radiative effects, which are not taken into account in these atmospheric models, therefore modify the dynamical as well as the photochemical results of the model simulations. Despite the importance of the actinic flux, the impact of 3-D atmospheric radiative transfer on the actinic flux within inhomogeneous cloud fields has been studied only recently [*Los et al.*, 1997; *Trautmann et al.*, 1999; *Vogelmann et al.*, 2001].

[11] The numerical methods of 3-D radiative transfer nowadays used in atmospheric sciences have first been developed for application to radiative gas dynamics and neutron transport in nuclear reactors [e.g., *Marchuk and Lebedev*, 1986]. The most common type of 3-D radiative transfer models use the Monte Carlo technique [e.g., *Marchuk et al.*, 1980; *Podgorny et al.*, 1998; *O'Hirok and Gautier*, 1998a]. These models simulate the transfer and fate of a single photon within the model domain. By repeating this calculation for a large number of photons, radiative quantities are derived with good accuracy. An alternative approach is the explicit calculation of the radiation field with a numerical solution method as commonly performed in 1-D radiative transfer simulations. An overview of explicit 3-D radiative transfer models is given by *Gabriel et al.* [1993]. The advantage of explicit methods is the calculation of the complete atmospheric radiation field at one time. This allows the determination of several radiative quantities without any extra effort.

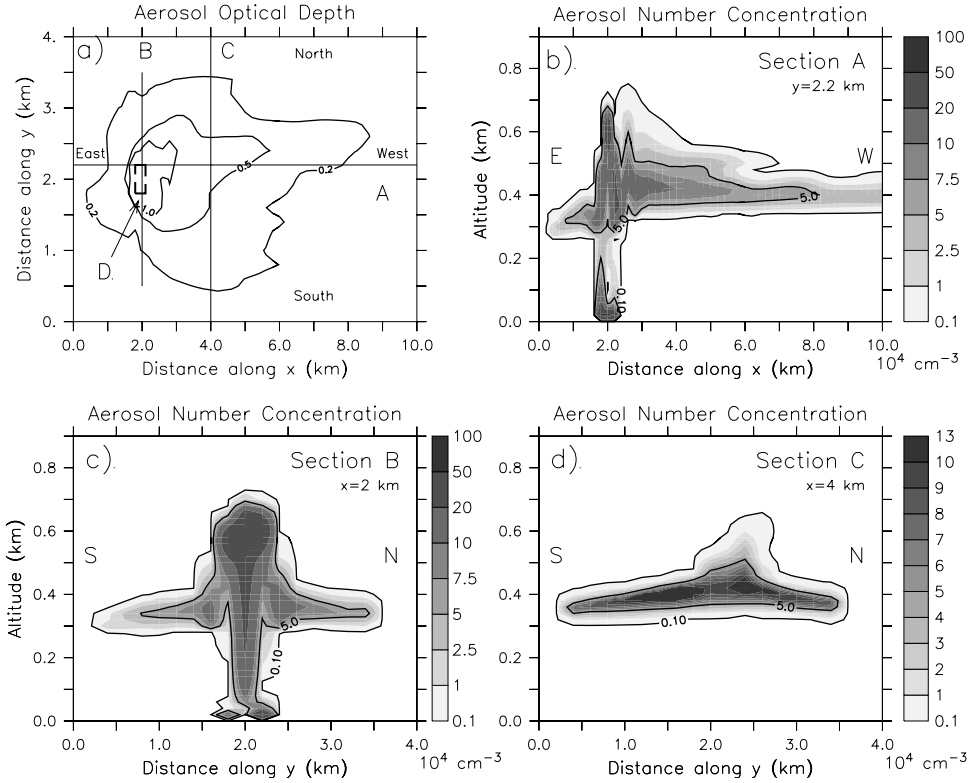

Figure 1. (a) Horizontal distribution of the aerosol optical depth at λ = 500 nm. The cross sections (A, B, and C) and the plume center (D), are also depicted. The fire is located inside box D. Cross sections of the aerosol number concentration (10^4 cm^{-3}) as gray scale and additionally as contour lines (b) along the plume at y = 2.2 km (cross section A), (c) across the plume at x = 2 km (cross section B), and (d) across the plume at x = 4 km (cross section C).

[12] In the present work, the spherical harmonics discrete ordinate method (SHDOM) [*Evans*, 1998], which belongs to the latter group of models, is used. SHDOM agrees well with Monte Carlo models for the zenith upwelling radiance, the up- and downwelling irradiance [*Evans*, 1998] and the actinic flux [*Trautmann et al.*, 1999] for inhomogeneous cloud fields. It has been used in several studies of 3-D radiation effects, including the effect of inhomogeneous clouds on atmospheric UV transmittance [*Meerkötter and Degünther*, 2001] and the effect of broken cloud fields on surface photolysis frequencies [*Junkermann et al.*, 2002]. Recently, it has been used to simulate actinic fluxes and photolysis frequencies in the presence of a convective cloud [*Brasseur et al.*, 2002]. In the present study, SHDOM will be used to simulate the atmospheric radiation field in the presence of a biomass-burning plume. Results from SHDOM for the actinic flux in the plume center are presented and compared to l-1-D simulations in order to investigate and quantify the 3-D radiation effects.

2. Scenario for the Radiative Transfer Modeling

[13] In this section, details of the model simulations, i.e., the spatial aerosol distribution, aerosol optical properties, and the model parameters, are presented.

[14] The spatial distribution of the aerosol particles is taken from a 3-D atmospheric transport simulation with the active tracer high-resolution atmospheric model (ATHAM) [*Oberhuber et al.*, 1998; *Trentmann et al.*, 2002]. This simulation reproduced the evolution of the biomass-burning plume from the Quinault prescribed fire during the Smoke, Cloud, and Radiation-C (SCAR-C) experiment on 21 September 1994. This 19.4 ha clearcut burn on the Pacific Coast of Washington state on the Olympic Peninsula and the resulting aerosol plume were intensively studied by remote sensing and in situ measurements [*Kaufman et al.*, 1996; *Hobbs et al.*, 1996; *Martins et al.*, 1996; *Tanré et al.*, 1997; *Gassó and Hegg*, 1998].

[15] The distribution of the aerosol optical depth as well as the aerosol number concentrations along three cross sections through the simulated spatial aerosol distribution 90 min after ignition are shown in Figure 1. ATHAM was able to reproduce the observed injection height of the aerosols (between 300 m and 700 m) as well as the horizontal extent of the plume from the Quinault fire reasonably well [*Trentmann et al.*, 2002]. The distinct aerosol plume with a width between 3 and 4 km was transported westward over the Pacific Ocean. Discrepancies between the observations and the simulated aerosol plume are an underestimation of the aerosol mass concentration as well as a too short total traveled distance [*Trentmann et al.*, 2002].

[16] The total model domain for the SHDOM simulations was set to 12 km in east-west direction (x direction), 4 km in south-north direction (y direction), and 60 km in the vertical direction. For the spatial discretization within SHDOM, a model domain of 60 grid cells in the east-west direction, 20 grid cells in the south-north direction and 59 grid cells

in the vertical direction was employed. The spatial resolution in the horizontal directions was 200 m, and 20 m in the vertical up to an altitude of 700 m. Since essentially all of the plume was situated within this altitude range, the properties of the plume and its heterogeneity could be reproduced. Above 700 m, the resolution was decreased to maximum 20 km at an altitude of 60 km. The spatial distribution of the aerosol from the original ATHAM simulation was linearly interpolated onto the grid used in SHDOM.

[17] For the aerosol particles, two different optical models are employed, A_{CON} and A_{ABS}. A_{ABS} relies on the same optical properties as in the dynamical ATHAM simulation [*Trentmann et al.*, 2002]. They are based on measurements of the size distribution and the chemical composition of the aerosol during the Quinault fire [*Martins et al.*, 1996; *Gassó and Hegg*, 1998]. A bimodal lognormal number size distribution with the effective radius $r_{eff} = 0.14$ μm and a black carbon mass content of 8% yield a value for the single-scattering albedo at $\lambda = 550$ nm of $\omega = 0.85$ calculated from Mie-Theory. This value for the single-scattering albedo corresponds to a rather high aerosol absorption, but it is a reasonable value for biomass burning aerosol [*Hobbs et al.*, 1996; *Reid et al.*, 1998]. In order to investigate the impact of aerosol absorption, a second aerosol model (A_{CON}) is defined assuming conservative scattering, i.e., the scattering coefficient is set to the extinction coefficient of the A_{ABS} aerosol model. In this way both aerosol models have the same extinction while the single-scattering albedo of A_{CON} is unity at all wavelengths. For both aerosol models, the phase function is approximated from the asymmetry parameter using the Henyey-Greenstein function, which was expanded into Legendre polynomials. The use of the Henyey-Greenstein function for aerosol particles instead of the Mie phase function is expected to result in only small differences for the simulated actinic flux [*van de Hulst*, 1981; *Boucher*, 1998] The wavelength dependent values for the single-scattering albedo and the asymmetry parameter are given in Table 1.

[18] Profiles for the meteorological data (temperature and pressure) and the ozone concentration were taken from the compilation for the standard atmosphere under midlatitude summer conditions [*Anderson et al.*, 1986]. These vertical profiles are assumed to be horizontally homogeneous. In order to easily identify the three-dimensional radiative effects of the biomass-burning plume in the simulations, the surface albedo was set to zero at all wavelengths.

[19] For the spectral extraterrestrial flux density the solar ATLAS-3 spectrum (available at http://wwwsolar.nrl.navy.mil/susim.html) was taken for $\lambda = 320$ and 400 nm. For wavelengths $\lambda = 550$ and 800 nm the values of the *World Meteorological Organization* [1985] were employed. The spectral extraterrestrial flux density was integrated to represent a wavelength bin of $\Delta\lambda = 1$ nm for $\lambda = 320$ nm, and $\Delta\lambda = 5$ nm for the other wavelengths.

[20] The spectral radiation transfer equation was solved for the wavelengths $\lambda = 320$, 400, 550, and 800 nm. The solar azimuth was set to 90°, leading to an illumination of the plume from the south. The simulations were carried out for 5 solar zenith angles (SZA): $\theta = 0°$, 30°, 45°, 60°, and 70°. The actinic flux was calculated using the 3-D model setup with 8 streams in zenith and 16 streams in azimuth direction. Lateral boundary conditions were assumed to be open so that outside the model domain no aerosol is assumed to exist. The cell splitting accuracy for the adaptive grid method implemented in SHDOM was set to 0.025 and the solution accurancy for the iteration was chosen to be 10^{-4}. Local 1-D simulations have also been performed using SHDOM with the same setup. Under homogeneous atmospheric conditions, the SHDOM l-1-D and 3-D results of the actinic flux agree within 1 to 2% [*Trautmann et al.*, 1999].

Table 1. Values of the Single-Scattering Albedo (ω) and the Asymmetry Parameter (g) for the Absorbing (A_ABS) and the Nonabsorbing (A_CON) Aerosol Models

	A_ABS		A_CON	
λ, nm	ω	g	ω	g
320	0.85	0.70	1.0	0.60
400	0.86	0.69	1.0	0.58
550	0.85	0.61	1.0	0.52
800	0.81	0.49	1.0	0.40

[21] The FORTRAN code of SHDOM is parallelized over the wavelengths and the simulations were performed on a Hewlett-Packard Superdome V-2500 parallel computer with 32 PA8500/440 MHz processors, each of them employing 1 GB of memory. The standard 3-D simulation used 4 processors (one for each wavelength) each requiring a memory of 950 MB and took about 9 min per solar zenith angle. Parallelization was performed using the message passing interface (MPI), HP MPI Version 1.07, software.

[22] For the following discussion of the model results, some abbreviations are introduced. Every model simulation is characterized by the kind of approximation (3-D or l-1-D) as well as the aerosol model used (CON, ABS). For instance, the 3-D simulation using the conservative aerosol model is called 3-D_CON. Additionally, some comparisons are presented for the clear sky case: NOAERO.

[23] In the following sections, relative differences between different model simulations for different radiative quantities are presented. The definition of all the relative differences (%) is

$$\Delta F(A) = \left(\frac{F(REF) - F(A)}{F(A)}\right) \times 100 \quad , \tag{1}$$

the letter A stands for the simulation NOAERO, l-1-D_CON, l-1-D_ABS, 3-D_CON, or 3-D_ABS. F is the actinic flux, which is defined in the following section.

3. Impact on the Actinic Flux

[24] The actinic flux is the radiative measure which quantifies photodissociation of atmospheric molecules [*Madronich*, 1987] and is therefore a critical parameter for photochemistry. It is defined as the integral of the radiance over the unit sphere and includes direct as well as diffuse radiation:

$$F(\lambda, z) = \int_0^{2\pi} \int_{-1}^{+1} L(\lambda, z, \mu, \varphi) d\mu d\varphi \, , \tag{2}$$

where $L(\lambda, z, \mu, \varphi)$ is the spectral radiance at the wavelength λ, μ the cosine of the zenith angle θ, φ the azimuth angle,

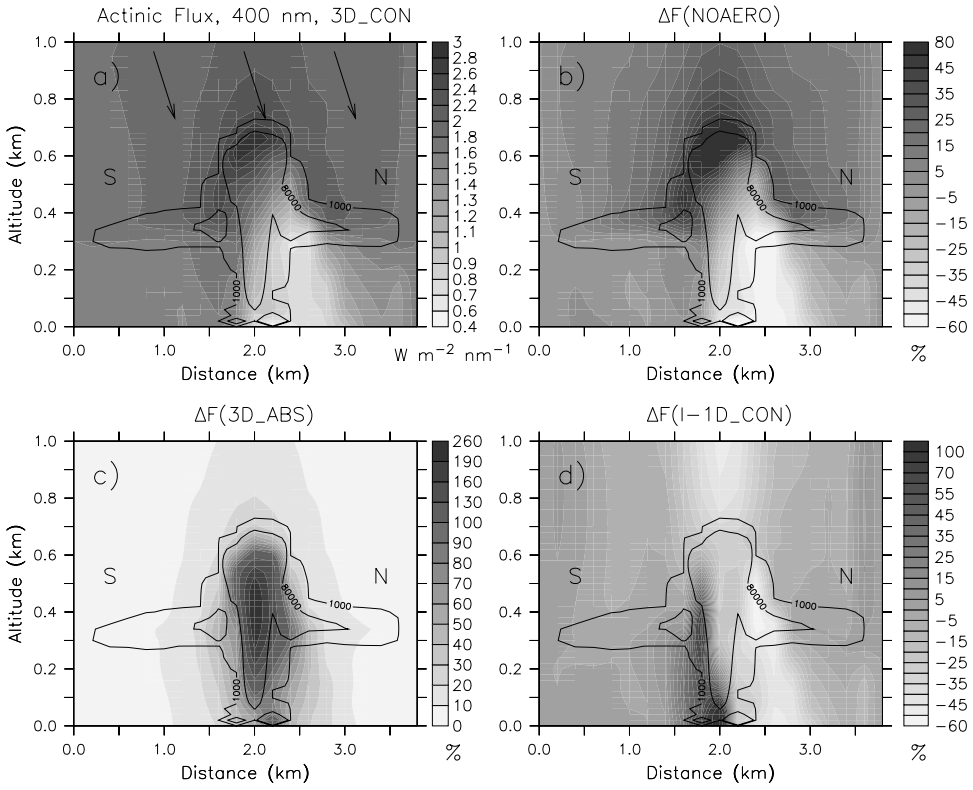

Figure 2. (a) Cross section (at section B) of the simulated actinic flux (W m^{-2} nm^{-1}) at λ = 400 nm using the A_{con} aerosol model for a SZA of 45° across the aerosol plume (x = 2 km). The arrows represent the solar illumination. The other plots show (b) ΔF(NOAERO), (c) ΔF(3-D_ABS), and (d) ΔF(l-1-D_CON) (REF = 3-D_CON for all differences) as color scale. Contour lines represent the aerosol number concentration (cm^{-3}). See color version of this figure at back of this issue.

and z the altitude. In sections 3.1–3.5, 3-D radiation effects on the actinic flux in the biomass-burning plume will be presented.

3.1. General Impact of the Aerosol

[25] In this section, the general impact of the biomass-burning plume, as well as the effect of the absorbing properties on the actinic flux is investigated. Finally, a comparison between 3-D and l-1-D results is presented.

[26] Figure 2a presents the actinic flux at λ = 400 nm along cross section B (defined in Figure 1a) through the center of the fire in the north-south direction calculated with the 3-D_CON simulation for a SZA θ = 45°. The relative difference of the actinic flux between the 3-D_CON and the NOAERO simulation, ΔF(NOAERO) (REF = 3-D_CON), is presented in Figure 2b. The effects of the aerosol plume on the radiation field are obvious. While the actinic flux is strongly reduced within and below the plume (up to −61%), it is enhanced (up to +82%) in the upper part of and above the plume as compared to the simulation without aerosol. It is interesting to note that the strongest reduction in the actinic flux does not occur in the center of the plume but is shifted to the north. This is due to the shadowing of the direct solar beam by the plume. In Figure 2c, ΔF (3-D_ABS) (REF = 3-D_CON) is shown, representing the impact of aerosol absorption on the actinic flux. The differences remain relatively small outside the center of the plume but increase to more than +200% within the plume center. This indicates the importance of the correct representation of aerosol absorption for radiative transfer simulations and atmospheric photochemistry.

[27] In Figure 2d the relative difference between the actinic flux calculated with the 3-D_CON and the l-1-D_CON simulations, ΔF(l-1-D_CON) (REF = 3-D_CON), is shown representing the differences due to horizontal photon transport in the 3-D simulations. F(l-1-D_CON) exceeds F(3-D_CON) in the upper part of the plume as well as above the plume significantly. For this scenario, horizontal photon transfer results in a loss of photons from the plume. As this process is not taken into account in the l-1-D simulation, it overestimates the actinic flux in this region. In the lower part of the plume, a dipole-like structure with an underestimation of the actinic flux in the l-1-D_CON simulation on the illuminated side of the plume (south) and an overestimate on the other side and behind the plume can be observed. The neglect of side illumination and the shadowing effect of the plume in the l-1-D_CON simulation is the reason for this structure. The maximum and minimum values of ΔF(l-1-D_CON) for the presented cross section are +128% and −55%, respectively.

[28] More than 2 km downwind the fire, the differences in the actinic flux, ΔF(l-1-D_CON), are comparably low (<5% within and below the plume, <15% above the plume, not shown here), because the optical depth of the plume is small and its structure shows only minor 3-dimensional

features. Large differences only occur close to the fire and near the center of the plume. The high aerosol numbers, together with their horizontally inhomogeneous distribution, increase the importance of 3-D radiation effects.

[29] The general effect of aerosol particles, as well as the aerosol absorption on the actinic flux and on photochemistry, have already been discussed in the literature [*Dickerson et al.*, 1997; *Jacobson*, 1998; *Liao et al.*, 1999; *He and Carmichael*, 1999]. Therefore we focus in the following on the effects of 3-D radiative transfer simulations on the atmospheric actinic flux.

3.2. Actinic Flux in the Center of the Plume

[30] As shown before, the center of the plume exhibits the largest 3-D radiation effects on the actinic flux. Additionally, this region is of special importance for photochemical processes, because here the concentrations of trace gases emitted by the fire (e.g., CO, NO, HCHO) are extremely high, reaching up to some 10 ppm for CO and some 100 ppb for NO_x (= NO + NO_2) [*Ward et al.*, 1992; *Hobbs et al.*, 1996; *Goode et al.*, 2000]. In this part of the plume, sunlight is the limiting factor for photochemistry.

[31] In Figure 3 we present the horizontal average of the actinic flux over the plume center, $\langle F \rangle_{pc}$ (where $\langle\ \rangle_{pc}$ denotes the horizontally averaging over the plume center) for the 3-D_CON and l-1-D_CON simulations at a SZA of $\theta = 45°$ and $\lambda = 400$ nm. The averaging only considers grid boxes in the column above the fire defined by the rectangle with x = 1.8 km to 2.1 km, y = 1.8 km to 2.2 km (box D in Figure 1a) where the aerosol number concentration exceeds 80,000 particles cm^{-3}.

[32] For the conservative aerosol model (Figure 3a), $\langle F$(l-1-D_CON)$\rangle_{pc}$ exceeds $\langle F$(3-D_CON)$\rangle_{pc}$ at nearly all altitudes. This can be explained by the horizontal photon transfer out of the plume center in the 3-D_CON simulation which is not taken into account in the l-1-D simulation. Photons scattered horizontally by aerosol particles escape from the region of the smoke plume. In the l-1-D case, no horizontal loss or gain of photons is considered. The vertically averaged difference between the 3-D and the l-1-D simulations for this case is $\overline{\Delta \langle F(\text{l-l-D\_CON}) \rangle_{pc}}$ (REF = 3-D_CON) = −14% (the bar represents the vertical average).

[33] In Figure 3b, the horizontally averaged actinic fluxes within the center of the plume are shown for the case of the absorbing aerosol model, $\langle F$(3-D_ABS)$\rangle_{pc}$ and $\langle F$(l-1-D_ABS)$\rangle_{pc}$. This is the more realistic case for a biomass-burning plume. For both cases the values are much lower than in the simulations using the conservative aerosol model. The differences between 3-D_ABS and l-1-D_ABS are distinct: $\langle F$(3-D_ABS)$\rangle_{pc}$ exceeds $\langle F$(l-1-D_ABS)$\rangle_{pc}$, especially in the lower part of the plume up to an altitude of about 600 m. While in the l-1-D_ABS simulation the actinic flux goes nearly to zero below the plume (0.09 W m^{-2} nm^{-1} at z = 200 m), the 3-D_ABS simulation gives a significant value for the actinic flux (0.54 W m^{-2} nm^{-1} at z = 200 m). This behavior can be explained by a net horizontal transport of photons into the plume center from regions with low aerosol loading which cannot be taken into account in the l-1-D simulation. Two processes account for the horizontal transfer of photons: direct illumination of the plume center from the side and the scattering from regions with lower aerosol loading into the plume center. In the plume center, the vertical optical depth and the absorption are very high (maximum: $\tau_{max} = 8.1$, average: $\tau_{ave} = 5.2$ at $\lambda = 550$ nm) leading to the strong reduction of radiation in the plume center in the l-1-D_ABS simulation. In the 3-D_ABS simulation, the direct solar radiation is not attenuated by this large optical depth, but is affected by a much smaller optical depth along its way to the plume center, because of the lateral illumination of the smoke plume. Additionally, Rayleigh scattering from regions outside the plume center into the plume enhances the actinic flux inside the plume. Although there is no spatial inhomogeneity in the distribution of molecules that are responsible for Rayleigh scattering, there is a net flux into the plume, because the number of photons is much larger outside the plume, leading to net Rayleigh scattering into the plume center. The loss of photons from the plume center due to

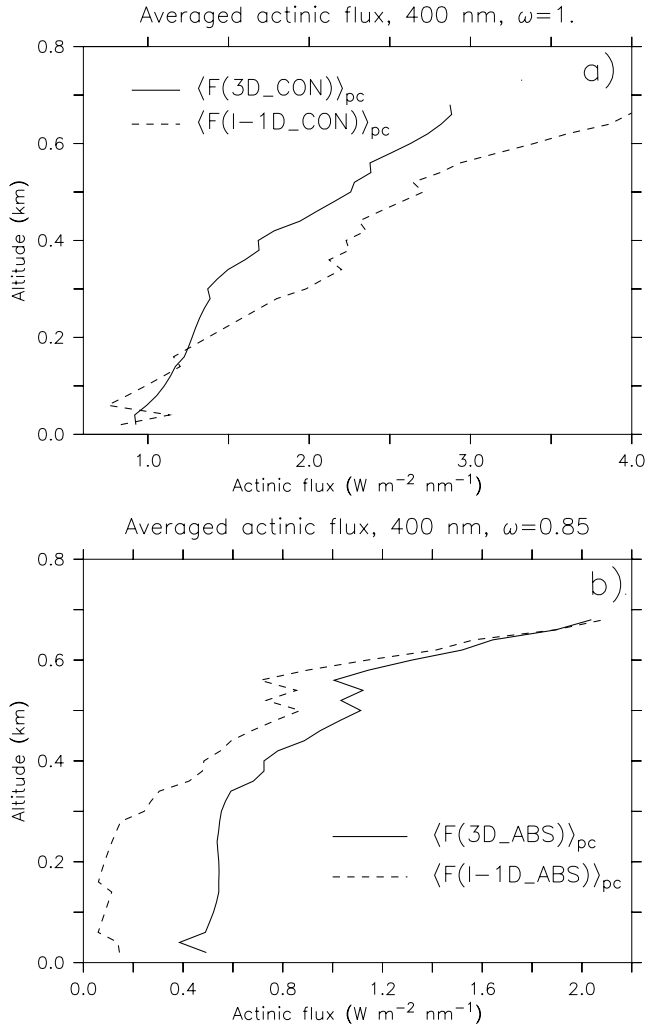

Figure 3. Horizontally averaged actinic flux (W m^{-2} nm^{-1}) at $\lambda = 400$ nm calculated for a SZA of 45°. The average includes only grid boxes with aerosol number concentrations higher than 80,000 particles cm^{-3} within box D (Figure 1a) representing the region very close to the fire. The top and bottom panels are for the purely scattering and absorbing aerosol models, respectively. Note the different scales on the abscissa.

Table 2. Differences in the Averaged Actinic Flux Within the Center of the Plume (Box D in Figure 1a) Between the 3-D_CON and the l-1-D_CON Simulations, $\overline{\Delta\langle F(\text{l-1-D\_CON})\rangle_{pc}}$ (REF = 3-D_CON), and the 3-D_ABS and the l-1-D_ABS Simulations, $\overline{\Delta\langle F(\text{l-1-D\_ABS})\rangle_{pc}}$ (REF = 3-D_ABS), for Different Wavelengths and Solar Zenith Angles[a]

	Wavelength, nm			
SZA	320	400	550	800
		$\overline{\Delta\langle F(\text{l-1-D\_CON})\rangle_{pc}}$		
0°	−42.9, −0.70, 0.90	−40.2, −1.37, 2.1	−43.4, −1.60, 2.15	−45.9, −0.91, 1.12
30°	−37.2, −0.51, 0.79	−29.8, −0.88, 1.94	−31.6, −1.03, 2.13	−35.0, −0.63, 1.16
45°	−31.0, −0.33, 0.63	−13.9, −0.40, 1.75	−11.5, −0.42, 2.01	−15.7, −0.3, 1.2
60°	−26.4, −0.17, 0.4	11.8, 0.03, 1.36	28.7, 0.23, 1.8	26.1, 0.12, 1.17
70°	−28.4, −0.11, 0.23	34.7, 0.17, 0.96	81.7, 0.53, 1.52	94.4, 0.4, 1.1
		$\overline{\Delta\langle F(\text{l-1-D\_ABS})\rangle_{pc}}$		
0°	155.8, 0.09, 0.35	62.4, 0.14, 0.95	8.93, −0.02, 1.29	−21.3, −0.21, 0.83
30°	209.7, 0.10, 0.31	116.7, 0.23, 0.91	42.2, 0.16, 1.29	−2.13, −0.06, 0.87
45°	281.6, 0.09, 0.25	214.2, 0.30, 0.84	111.5, 0.36, 1.27	38.0, 0.12, 0.91
60°	334.2, 0.06, 0.16	388.0, 0.32, 0.68	261.5, 0.54, 1.16	128.0, 0.33, 0.91
70°	323.0, 0.04, 0.09	530.8, 0.27, 0.48	460.1, 0.58, 0.98	285.6, 0.46, 0.86

[a]Shown are the averaged relative differences (%), the averaged absolute differences (W m^{-2} nm^{-1}), and the averaged absolute value of the actinic flux (W m^{-2} nm^{-1}) in the plume center from the 3-D simulation.

Mie scattering by the aerosol particles is comparably small because of the limited number of available photons. The averaged difference of the actinic flux in the plume center for this case, $\overline{\Delta\langle F(\text{l-1-D\_ABS})\rangle_{pc}}$ (REF = 3-D_ABS), is +214%.

[34] The three-dimensional radiation effects on the actinic flux are therefore distinctly different for the two aerosol models. In the case of the conservative aerosol, horizontal photon transfer leads to a reduction of the actinic flux. For the absorbing aerosol model, net horizontal photon transfer into the plume center enhances the actinic flux when three-dimensional radiation effects are considered.

3.3. Effect of Solar Zenith Angle and Wavelength on the Actinic Flux in the Plume Center

[35] In this section, we examine how the 3-D effects on the actinic flux in the plume center depend on solar zenith angle and wavelength.

[36] Table 2 presents the vertically averaged relative difference between the 3-D and the l-1-D simulation, together with the vertically averaged absolute difference. It also gives the averaged actinic flux in the plume center for the 3-D simulation at the 4 wavelengths and the five solar zenith angles studied. In Figure 4, we show the relative differences between the 3-D and the l-1-D simulations as functions of the wavelength and the solar zenith angle for the two aerosol models.

[37] In the case of the conservative aerosol, the actinic flux resulting from the l-1-D simulation is larger than the 3-D results ($\overline{\Delta\langle F(\text{l-l-D\_CON})\rangle_{pc}}$ (REF = 3-D_CON) < 0) at all wavelengths for solar zenith angles below 50°. $\overline{\Delta\langle F(\text{l-l-D\_CON})\rangle_{pc}}$ increases with increasing solar zenith angle, but depends only slightly on wavelength (Figure 4a).

[38] Horizontal photon transfer is responsible for the differences between the 3-D and the l-1-D simulations. For overhead sun, only scattering contributes to the horizontal photon transfer. Mie scattering is responsible for the horizontal photon transfer out of the plume center, which is not taken into account in the l-1-D simulations. As Mie scattering depends only slightly on wavelength, no significant change of the 3-D effect on the actinic flux in the plume center occurs as a function of wavelength. For larger SZAs, the direct solar radiation also contributes to the horizontal photon transfer into the plume center in the 3-D simulation and $\overline{\Delta\langle F(\text{l-1-D\_CON})\rangle_{pc}}$ increases at all wavelengths with increasing solar zenith angle. For wavelengths larger than 400 nm and solar zenith angles larger than 50°, the l-1-D simulation underestimates the actinic flux compared to the 3-D simulation. In the 3-D simulations, the direct solar radiation in the plume center is less attenuated at larger SZAs than in the l-1-D simulations, because the direct solar beam does not interact with the dense part of the plume above the fire but enters the plume center from the side. This effect dominates at all wavelengths where the direct solar radiation has a significant contribution to the actinic flux in the plume center. At short wavelengths ($\lambda < 400$ nm), the direct solar radiation at large SZAs is highly depleted due to Rayleigh scattering and ozone absorption. Therefore this effect is not as pronounced as at longer wavelengths and for 320 nm the l-1-D simulation of the actinic flux in the plume center is higher than the 3-D simulation for all SZA.

[39] In the case of the absorbing aerosol model, A_{ABS}, the values of $\overline{\Delta\langle F(\text{l-1-D\_ABS})\rangle_{pc}}$ (REF = 3-D_ABS) are much larger than the corresponding values for A_{CON}. In contrast to the simulations with the conservative aerosol, here the values of $\overline{\Delta\langle F(\text{l-1-D\_ABS})\rangle_{pc}}$ are positive in almost all cases, representing higher actinic flux in the plume center in the 3-D than in the l-1-D simulations. Because of the low actinic flux in the plume center, horizontal photon loss from the plume center due to Mie scattering is limited, and gain of photons due to side illumination and Rayleigh scattering makes a significant contribution to the total number of photons in the plume. This contribution is neglected in the l-1-D simulations, resulting in the reduced actinic flux in the plume center.

[40] At overhead sun, only horizontal scattering (Rayleigh and Mie) is responsible for the difference between the 3-D and the l-1-D simulation. At short wavelengths, Rayleigh scattering into the plume center enhances the actinic flux in the 3-D simulation. The strong wavelength dependence of

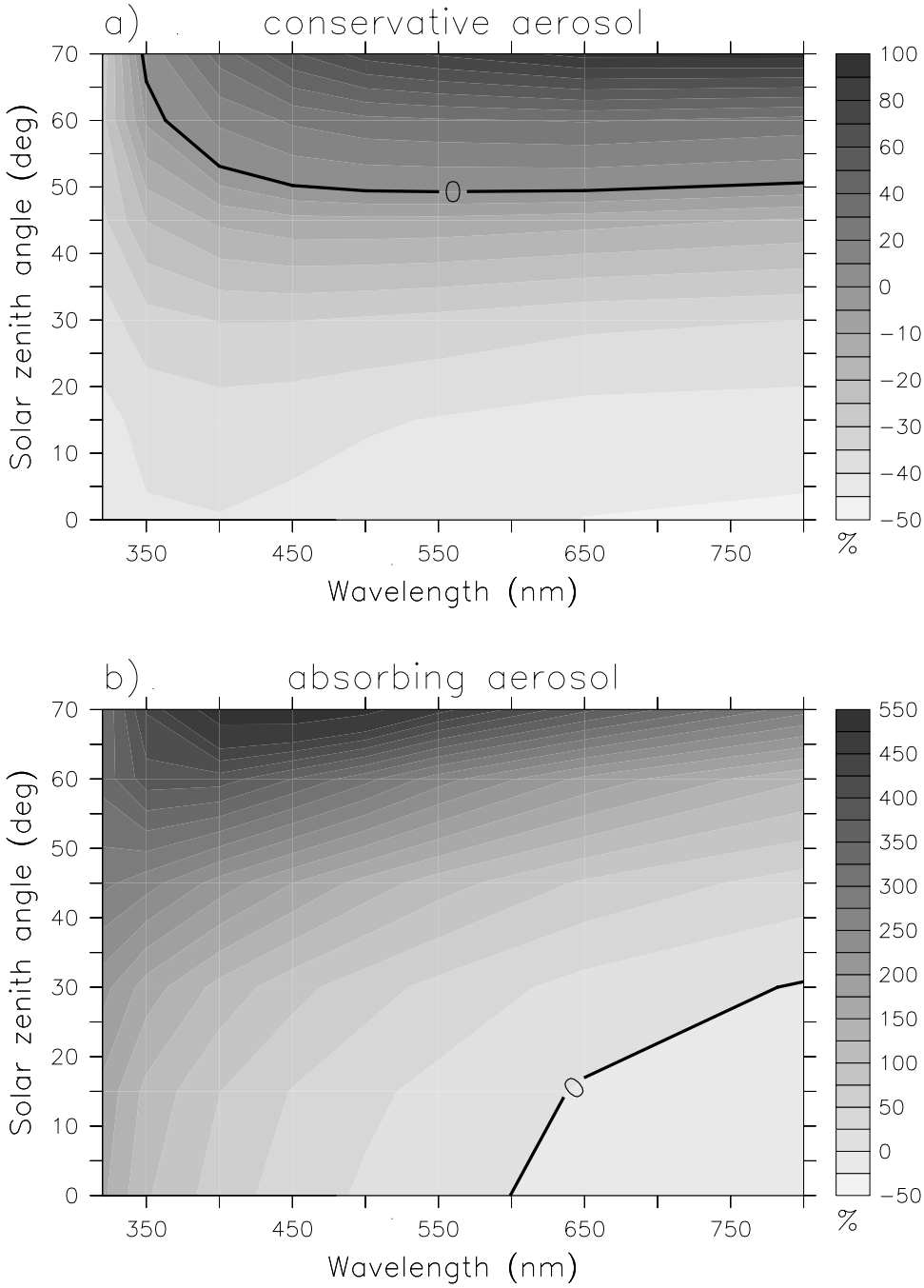

Figure 4. Contour plot of the relative difference of the actinic flux in the plume center between the 3-D and the l-1-D simulation as a function of wavelength and solar zenith angle for the conservative ($\overline{\Delta\langle F(\text{l-l-D\_CON})\rangle_{pc}}$ (REF = 3-D_CON)) (a) and the absorbing ($\overline{\Delta\langle F(\text{l-l-D\_ABS})\rangle_{pc}}$ (REF = 3-D_ABS)) (b) aerosol. For the preparation of these figures, values at a SZA of 15° and at wavelengths of 350, 450, 500, and 650 nm were included in addition to those of Table 2. See color version of this figure at back of this issue.

Rayleigh scattering results in a strong wavelength dependence of $\overline{\Delta\langle F(\text{l-l-D\_ABS})\rangle_{pc}}$. At longer wavelengths, horizontal Mie scattering out of the plume center dominates, leading to a lower actinic flux in the 3-D simulation for $\lambda >$ 600 nm at overhead sun.

[41] At larger SZAs, the contribution of the direct solar light in the plume center in the 3-D_ABS simulation increases, because of the illumination of the lateral plume faces. As the direct solar radiation is much less attenuated in the 3-D as compared to the l-1-D simulation, $\overline{\Delta\langle F(\text{l-l-D\_ABS})\rangle_{pc}}$ increases with increasing solar zenith angle and exceeds +100% at all wavelengths.

3.4. Sensitivity Studies

[42] In order to exclude the possibility that numerical errors might be responsible for the simulated 3-D radiation

Table 3. Averaged Relative Differences of the Actinic Flux in the Plume Center Between the 3-D and the l-1-D Simulations for Three Wavelengths, Three Solar Zenith Angles, and the Two Aerosol Models Evaluated for Three Sensitivity Simulations: Reference, Increased Horizontal Resolution, and Increased Number of Streams

	Wavelength, nm		
SZA	320	550	800
	$\overline{\Delta\langle F(l\text{-}1\text{-}D\_CON)\rangle_{pc}}$ (REF = 3-D_CON)		
0°	−42.9, −44.2, −42.7	−43.4, −46.0, −43.4	−45.9, −48.0, −46.0
45°	−31.0, −28.1, −31.0	−11.5, −2.4, −13.6	−15.7, −6.8, −16.1
70°	−28.4, −26.1, −28.0	81.7, 104.7, 93.1	94.4, 113.2, 93.1
	$\overline{\Delta\langle F(\text{l-1-D\_ABS})\rangle_{\text{pc}}}$ (REF = 3-D_ABS)		
0°	156, 178, 159	8.9, 6.9, 9.6	−21.3, −23.1, −21.4
45°	282, 373, 285	112, 161, 113	38.0, 60.3, 38.1
70°	323, 412, 325	460, 576, 466	286, 335, 285

effects, we performed two sensitivity studies: 1. we increased the horizontal resolution from 200 m to 100 m, and 2. we increased the number of streams in zenith and azimuth direction from 8 and 16 to 16 and 32, respectively.

[43] For these sensitivity simulations, the average relative difference of the actinic flux in the plume center between the corresponding 3-D and l-1-D simulations were calculated. The results are presented in Table 3 for the two aerosol models, three wavelengths and three SZAs together with the corresponding values from the reference simulation. The doubling of the number of streams in the calculation leads to only small changes in the resulting 3-D radiation effects. The increased horizontal resolution has a slightly larger impact on the relative differences. However, the dependence of the three-dimensional effects on wavelength and solar zenith angle shows the same behaviour as in the reference simulation. These studies show that our conclusions from section 3.3 are independent of the model configuration.

3.5. Possible Impact on Photochemistry

[44] The errors in the actinic flux due to the neglect of 3-D radiation effects translate directly into errors in the calculation of the atmospheric photolysis frequencies. The differences between the 3-D and the l-1-D simulations reported here are significantly larger than the uncertainties in the calculation of the photolysis frequency due to the use of different numerical methods and uncertainties in the measurements of aerosol parameters [*Früh et al.*, 2000]. These authors found the agreement between observed and simulated NO_2 photolysis frequency to be within the intrumental uncertainty of the photolysis instrument (10 to 15%) [*Früh et al.*, 2000].

[45] Photodissociation of atmospheric molecules primarily occurs at wavelengths shorter than 420 nm. For these wavelengths, the results of this study show a strong variability of the effects of 3-D radiative transfer simulations, depending on the solar zenith angle and the absorbing properties of the aerosol particles. In the nonabsorbing case, for most SZAs the actinic flux and therefore the photolysis frequency is overestimated by l-1-D_CON simulations by +10 to +40% because of the neglect of horizontal photon loss. At larger SZAs, this effect is opposite due to solar side illumination. The magnitude of this effect is expected to depend strongly on the spatial dimensions of the plume considered. In the case of an absorbing aerosol, the available actinic flux for photodissociation is heavily underestimated by the l-1-D_ABS simulation in the cases considered here. It is not possible to give a general estimate of the error in the actinic flux due to the neglect of 3-D radiative transfer effects, because the strong impact of aerosol absorption, which can lead to an overestimation as well as to an underestimation of the actinic flux in l-1-D simulations. It is clear, however, that neglecting the 3-dimensional nature of radiative transfer in cloud- and plume-resolving photochemical models results in significant errors for the simulation of photolysis frequencies in many cases.

[46] How these errors in the simulated photolysis frequencies transfer into the simulation of photochemical processes, e.g., the formation of ozone in the troposphere, needs further investigation. Again, a general statement even for the sign of the 3-D impact is not possible, because photochemical ozone production strongly depends on the available NO_x concentration. However, under the conditions of a biomass-burning plume, i.e., absorbing aerosol and high concentrations of organic compounds and nitrogen oxides, the inclusion of 3-D radiation effects would lead to enhanced photolysis frequencies and enhanced photochemistry, including the formation of tropospheric ozone. Fast production of ozone and other trace gases within individual biomass-burning plumes has been reported several times [e.g., *Evans et al.*, 1977; *Hobbs et al.*, 1996, 2003; *Goode et al.*, 2000; *Yokelson et al.*, 2003; *Jost et al.*, 2003]. Three-dimensional radiation effects might contribute to the fast photochemistry appearing within these plumes. Also for the case of convective clouds, 3-D radiation effects might influence photochemistry.

4. Conclusions

[47] The impact of three-dimensional radiative transfer effects on the actinic flux in an aerosol plume from a vegetation fire was investigated. In order to quantify this effect, three-dimensional model simulations were compared with local one-dimensional (l-1-D) radiative transfer simulations assuming horizontal homogeneity for every model column. Horizontal photon transport due to direct illumination as well as horizontal scattering, which is not accounted for in the l-1-D simulations, is responsible for the difference between these two simulations.

[48] For the scenario investigated here the three-dimensional effect on the actinic flux within the plume center ranges from −40% to more than +200%, depending on the

solar zenith angle, the wavelength, and the absorbing properties of the aerosol. For a conservative aerosol, the loss of photons from the plume center due to horizontal scattering leads to an overestimation of the actinic flux in the l-1-D simulations for SZA smaller than about 50°. In the case of an absorbing aerosol, horizontal photon transfer into the plume center enhances the actinic flux in the plume at nearly all solar zenith angles and wavelengths in the 3-D simulations. The magnitude of the difference indicates the importance of three-dimensional radiative effects for photochemical processes within biomass-burning plumes and other 3-dimensional atmospheric structures, e.g., convective clouds. However, at present, 3-D radiative transfer models cannot be included in atmospheric chemistry models, because of their high computing time and memory requirements.

[49] Further investigations of 3-D radiation effects using both model simulations and measurements would be desirable. Our study shows that 3-D effects on the actinic flux and their potential impact on photochemistry need to be considered, and suitable parameterizations should be investigated.

[50] **Acknowledgments.** O.B. would like to thank Jos Lelieveld and the Max Planck Institute for Chemistry for hospitality. The authors wish to thank Frank Evans for providing his radiation code and advice on its use. This research was supported by the German Ministry for Education and Research (BMBF) under grant 07 ATF 46 (EFEU), the German Max Planck Society, the 'Zentrum für Umweltforschung' of the University of Mainz, and the Programme National de Télédétection Spatiale (PNTS) of the CNRS. The authors would like to acknowledge the support of the European Commission through TMR grant number ERB FMGE CT950051 (the TRACS Programme at EPCC). The simulations were carried out on the HP Superdome 750/32 of the ZDV, University of Mainz. The authors wish to acknowledge use of the Ferret program for analysis and graphics in this paper. Ferret is a product of NOAA's Pacific Marine Environmental Laboratory. (Information is available at http://www.ferret.noaa.gov) We thank the reviewers for their helpful comments.

References

Anderson, G. P., S. A. Clough, F. X. Kneizys, J. H. Chetwynd, and E. P. Shettle, AFGL atmospheric constituent profiles (0–120 km), *Tech. Rep. AFGL-TR-86-0110*, Air Force Geophys. Lab., Hanscom Air Force Base, Mass., 1986.

Benner, T. C., and K. F. Evans, Three-dimensional solar radiative transfer in small tropical cumulus fields derived from high-resolution imagery, *J. Geophys. Res.*, *106*, 14,975–14,984, 2001.

Borde, R., and H. Isaka, Radiative transfer in multifractal clouds, *J. Geophys. Res.*, *101*, 29,461–29,478, 1996.

Boucher, O., On aerosol direct shortwave forcing and the Henyey-Greenstein phase function, *J. Atmos. Sci.*, *55*, 128–134, 1998.

Brasseur, A.-L., R. Ramaroson, A. Delannoy, W. Skamarock, and M. Barth, Three-dimensional calculation of photolysis frequencies in the presence of clouds and impact on photochemistry, *J. Atmos. Chem.*, *41*, 211–237, 2002.

Cahalan, R. F., W. Rodgway, W. J. Wiscombe, T. L. Bell, and J. B. Snider, The albedo of fractal stratocumulus clouds, *J. Atmos. Sci.*, *51*, 2434–2455, 1994.

Cairns, B., A. A. Lace, and B. E. Charlson, Absorption within inhomogeneous clouds and its parameterization in general circulation models, *J. Atmos. Sci.*, *57*, 700–714, 2000.

Cess, R. D., et al., Absorption of solar radiation by clouds: Observations versus models, *Science*, *267*, 496–499, 1995.

Dickerson, R. R., S. Kondragunta, G. Stenchikov, K. L. Civerolo, B. G. Doddridge, and B. N. Holben, The impact of aerosols on solar ultraviolet radiation and photochemical smog, *Science*, *278*, 827–830, 1997.

Duynkerke, P., P. Jonker, A. C. M. van Zanten, J. Cuxart, P. Clark, E. Sanchez, G. Martin, G. Lenderink, and J. Teixeira, Intercomparison of three- and one-dimensional model simulations and aircraft observations of stratocumulus, *Boundary Layer Meteorol.*, *92*, 453–487, 1999.

Evans, K. F., The spherical harmonics discrete ordinate method for three-dimensional atmospheric radiative transfer, *J. Atmos. Sci.*, *55*, 429–446, 1998.

Evans, L. F., I. A. Weeks, A. J. Eccleston, and D. R. Packham, Photochemical ozone in smoke from prescribed burning of forests, *Environ. Sci. Technol.*, *11*, 896–900, 1977.

Ferrare, R. A., R. S. Fraser, and Y. J. Kaufman, Satellite measurements of large-scale air pollution: Measurements of forest fire smoke, *J. Geophys. Res.*, *95*, 9911–9925, 1990.

Früh, B., T. Trautmann, M. Wendisch, and A. Keil, Comparison of observed and simulated NO_2 photodissociation frequencies in a cloudless atmosphere and in continental boundary layer clouds, *J. Geophys. Res.*, *105*, 9843–9857, 2000.

Gabriel, P. M., S.-C. Tsay, and G. L. Stephens, A Fourier-Riccati approach to radiative transfer. part I: Foundations, *J. Atmos. Sci.*, *50*, 3125–3147, 1993.

Gassó, S., and D. A. Hegg, Comparison of columnar aerosol optical properties measured by the MODIS Airborne Simulator with in situ measurements: A case study, *Remote Sens. Environ.*, *66*, 138–152, 1998.

Goode, J. G., R. J. Yokelson, D. E. Ward, R. A. Susott, R. E. Babbitt, M. A. Davis, and W. M. Hao, Measurements of excess O_3, CO_2, CO, CH_4, C_2H_4, C_2H_2, HCN, NO, NH_3, HCOOH, CH_3COOH, HCHO, and CH_3OH in 1997 Alaskan biomass burning plumes by airborne Fourier transform infrared spectroscopy (AFTIR), *J. Geophys. Res.*, *105*, 22,147–22,166, 2000.

Halthore, R. N., and S. E. Schwartz, Comparison of model-estimated and measured diffuse downward irradiance at surface in cloud-free skies, *J. Geophys. Res.*, *105*, 20,165–20,177, 2000.

He, S., and G. R. Carmichael, Sensitivity of photolysis rates and ozone production in the troposphere to aerosol properties, *J. Geophys. Res.*, *104*, 26,307–26,324, 1999.

Hobbs, P. V., J. S. Reid, J. A. Herring, J. D. Nance, R. E. Weiss, J. L. Ross, D. A. Hegg, R. D. Ottmar, and C. Liousse, Particle and trace-gas measurements in the smoke from prescribed burns of forest products in the Pacific Northwest, in *Biomass Burning and Global Change*, edited by J. S. Levine, pp. 697–715, MIT Press, Cambridge, Mass., 1996.

Hobbs, P. V., P. Sinha, R. J. Yokelson, T. J. Christian, D. R. Blake, S. Gao, T. W. Kirchstetter, T. Novakov, and P. Pilewskie, Evolution of gases and particles from a savanna fire in South Africa, *J. Geophys. Res.*, *108*(D13), 8485, doi:10.1029/2002JD002352, 2003.

Jacobson, M. Z., Studying the effect of aerosols on vertical photolysis rate coefficient and temperature profiles over an urban airshed, *J. Geophys. Res.*, *103*, 10,593–10,604, 1998.

Jost, C., J. Trentmann, D. Sprung, M. O. Andreae, J. B. McQuaid, and H. Barjat, Trace gas chemistry in a young biomass burning plume over Namibia: Observations and model simulations, *J. Geophys. Res.*, *108*(D13), 8482, doi:10.1029/2002JD002431, 2003.

Junkermann, W., et al., Actinic radiation and photolysis processes in the lower troposphere: Effect of clouds and aerosols, *J. Atmos. Chem.*, *42*, 413–441, 2002.

Kato, S., T. P. Ackermann, E. E. Clothiaux, J. H. Mather, G. G. Mace, M. L. Wesely, F. Murcray, and J. Michalsky, Uncertainties in modeled and measured clear-sky surface shortwave irradiances, *J. Geophys. Res.*, *102*, 25,881–25,898, 1997.

Kaufman, Y. J., et al., Relationship between remotely sensed fire intensity and rate of emission of smoke: SCAR-C experiment, in *Biomass Burning and Global Change*, edited by J. S. Levine, pp. 685–696, MIT Press, Cambridge, Mass., 1996.

Khairoutdinov, M. F., and D. A. Randall, Cloud resolving modeling of the ARM summer 1997 IOP: Model formulation, results, uncertainties, and sensitivities, *J. Appl. Meteorol.*, *60*, 607–625, 2003.

Liao, H., Y. L. Yung, and J. H. Seinfeld, Effects of aerosols on tropospheric photolysis rates in clear and cloudy atmospheres, *J. Geophys. Res.*, *104*, 23,697–23,707, 1999.

Liousse, C., C. Devaux, F. Dulac, and H. Cachier, Aging of savanna biomass burning aerosols: Consequences on their optical properties, *J. Atmos. Chem.*, *22*, 1–17, 1995.

Los, A., M. van Weele, and P. G. Duynkerke, Actinic fluxes in broken cloud fields, *J. Geophys. Res.*, *102*, 4257–4266, 1997.

Lu, R., C. Lin, R. Turco, and A. Arakawa, Cumulus transport of chemical tracers: 1. Cloud-resolving model simulations, *J. Geophys. Res.*, *105*, 10,001–10,021, 2000.

Lyapustin, A. I., and Y. J. Kaufman, Role of adjacency effect in the remote sensing of aerosol, *J. Geophys. Res.*, *106*, 11,909–11,916, 2001.

Madronich, S., Photodissociation in the atmosphere: 1. Actinic flux and effects of ground reflections and clouds, *J. Geophys. Res.*, *92*, 9740–9752, 1987.

Marchuk, G. I., and V. I. Lebedev, *Numerical Methods in the Theory of Neutron Transport*, Harwood Acad., New York, 1986.

Marchuk, G. I., G. A. Mikhailiv, M. A. Nazaraliev, R. A. Darbinjan, B. A. Kargina, and B. S. Elepov, *The Monte Carlo Methods in Atmospheric Optics*, *Springer Ser. Opt. Sci.*, vol. 12, Springer-Verlag, New York, 1980.

Marshak, A., A. Davis, W. Wiscombe, and R. Cahalan, Radiative smoothing in fractal clouds, *J. Geophys. Res.*, *100*, 26,247–26,261, 1995.

Martins, J. V., P. Artaxo, P. V. Hobbs, C. Liousse, H. Cachier, Y. Kaufman, and A. Plana-Fattori, Particle size distribution, elemental composition, carbon measurements, and optical properties of smoke from biomass burning in the Pacific Northwest of the United States, in *Biomass Burning and Global Change*, edited by J. S. Levine, pp. 716–732, MIT Press, Cambridge, Mass., 1996.

Meerkötter, R., and M. Degünther, A radiative transfer case study for 3-D cloud effects in the UV, *Geophys. Res. Lett.*, *28*, 1683–1686, 2001.

Oberhuber, J. M., M. Herzog, H.-F. Graf, and K. Schwanke, Volcanic plume simulation on large scales, *J. Volcanol. Geotherm. Res*, *87*, 29–53, 1998.

O'Hirok, W., and C. Gautier, A three-dimensional radiative transfer model to investigate the solar radiation within a cloudy atmosphere. part I: Spatial effects, *J. Atmos. Sci.*, *55*, 2162–2179, 1998a.

O'Hirok, W., and C. Gautier, A three-dimensional radiative transfer model to investigate the solar radiation within a cloudy atmosphere. part II: Spectral effects, *J. Atmos. Sci.*, *55*, 3065–3076, 1998b.

Podgorny, I. A., A. M. Vogelmann, and V. Ramanathan, Effects of cloud shape and water vapor distribution on solar absorption in the near-infrared, *Geophys. Res. Lett.*, *25*, 1899–1902, 1998.

Ramanathan, V., B. Subasilar, G. J. Zhang, W. Conant, R. D. Cess, J. T. Kiehl, H. Grassl, and L. Shi, Warm pool heat budget and shortwave cloud forcing: A missing physics?, *Science*, *267*, 499–503, 1995.

Reid, J. S., P. V. Hobbs, R. J. Ferek, D. R. Blake, J. V. Martins, M. R. Dunlap, and C. Liousse, Physical, chemical, and optical properties of regional hazes dominated by smoke in Brazil, *J. Geophys. Res.*, *103*, 32,059–32,080, 1998.

Skamarock, W. C., et al., Numerical simulations of the July 10 Stratospheric-Tropospheric Experiment: Radiation, Aerosols, and Ozone/Deep Convection Experiment convective system: Kinematics and transport, *J. Geophys. Res.*, *105*, 19,973–19,990, 2000.

Stevens, B., et al., Simulations of trade wind cumuli under a strong inversion, *J. Atmos. Sci.*, *58*, 1870–1891, 2001.

Tanré, D., Y. J. Kaufman, M. Herman, and S. Mattoo, Remote sensing of aerosol properties over oceans using the MODIS/EOS spectral radiances, *J. Geophys. Res.*, *102*, 16,971–16,988, 1997.

Trautmann, T., I. Podgorny, J. Landgraf, and P. J. Crutzen, Actinic fluxes and photodissociation coefficients in cloud fields embedded in realistic atmospheres, *J. Geophys. Res.*, *104*, 30,173–30,192, 1999.

Trentmann, J., M. O. Andreae, H.-F. Graf, P. V. Hobbs, R. D. Ottmar, and T. Trautmann, Simulation of a biomass-burning plume: Comparison of model results with observations, *J. Geophys. Res.*, *107*(D2), 4013, doi:10.1029/2001JD000410, 2002.

van de Hulst, H., *Light Scattering by Small Particles*, Dover, Mineola, N. Y., 1981.

Várnai, T., and R. Davis, Effects of cloud heterogeneities on shortwave radiation: Comparison of cloud-top variabiliy and internal heterogeneity, *J. Atmos. Sci.*, *56*, 4206–4224, 1999.

Vilà-Guerau de Arellano, J., and J. W. M. Cuijper, The chemistry of a dry cloud: The effect of radiation and turbulence, *J. Atmos. Sci.*, *57*, 1573–1584, 2000.

Vogelmann, A. M., V. Ramanathan, and I. A. Podgorny, Scale dependence of solar heating rates in convective cloud systems with implications to general circulation models, *J. Clim.*, *14*, 1738–1752, 2001.

Wang, C., and R. G. Prinn, On the roles of deep convective clouds in tropospheric chemistry, *J. Geophys. Res.*, *105*, 22,269–22,297, 2000.

Ward, D. E., et al., Smoke and fire characteristics for cerrado and deforestation burns in Brazil: BASE-B experiment, *J. Geophys. Res.*, *97*, 14,601–14,619, 1992.

Wild, M., Discrepancies between model-calculated and observed shortwave atmospheric absorption in areas with high aerosol loadings, *J. Geophys. Res.*, *104*, 27,361–27,371, 1999.

World Meteorological Organization, Atmospheric Ozone, *Rep.16*, Global Ozone Res. and Monit. Proj., Geneva, Switzerland, 1985.

Xu, K.-M., and D. A. Randall, Impact of interactive radiative transfer on the macroscopic behavior of cumulus ensembles. part I: Radiation parameterization and sensitivity tests, *J. Appl. Meteorol.*, *52*, 785–799, 1995.

Yokelson, R. J., I. T. Bertschi, T. J. Christian, P. V. Hobbs, D. E. Ward, and W. M. Hao, An overview of trace gas measurements in nascent, aged, and cloud-processed smoke from African savanna fires by airborne Fourier transform infrared spectroscopy, *J. Geophys. Res.*, *108*(D13), 8478, doi:10.1029/2002JD002322, 2003.

M. O. Andreae, Department of Biogeochemistry, Max Planck Institute for Chemistry, P.O. Box 3060, D-55020 Mainz, Germany. (andreae@mpch-mainz.mpg.de)

O. Boucher, Laboratoire d'Optique Atmosphérique, UFR de Physique, Bat P5, Université des Sciences et Technologies de Lille, 59655 Villeneuve d'Ascq, France. (boucher@loa.univ-lille1.fr)

B. Früh, Institute for Atmospheric Physics, University of Mainz, Becherweg 21, 55128 Mainz, Germany. (frueh@uni-mainz.de)

T. Trautmann, Institut für Methodik der Fernerkundung, Deutsches Zentrum für Luft- und Raumfahrt e.V. (DLR), Oberpfaffenhofen, 82234 Wessling, Germany. (thomas.trautmann@dlr.de)

J. Trentmann, Department of Atmospheric Sciences, University of Washington, Box 351640, Seattle, WA 98195-1640, USA. (jtrent@atmos.washington.edu)

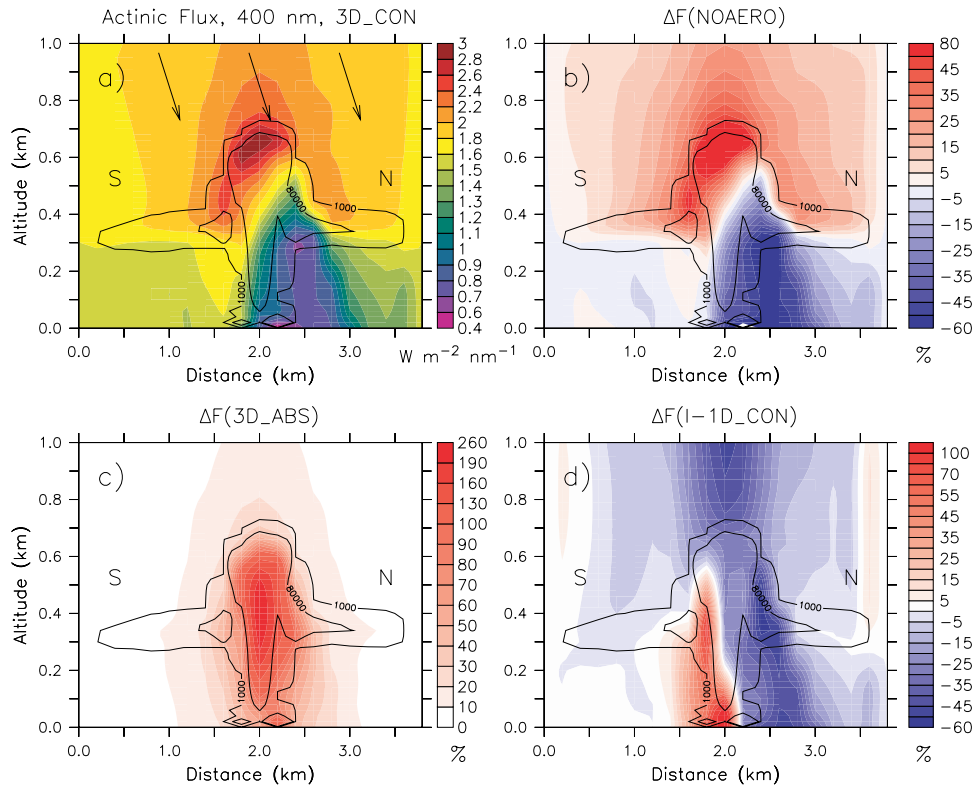

Figure 2. (a) Cross section (at section B) of the simulated actinic flux (W m^{-2} nm^{-1}) at λ = 400 nm using the A_{con} aerosol model for a SZA of 45° across the aerosol plume (x = 2 km). The arrows represent the solar illumination. The other plots show (b) ΔF(NOAERO), (c) ΔF(3-D_ABS), and (d) ΔF(l-1-D_CON) (REF = 3-D_CON for all differences) as color scale. Contour lines represent the aerosol number concentration (cm^{-3}).

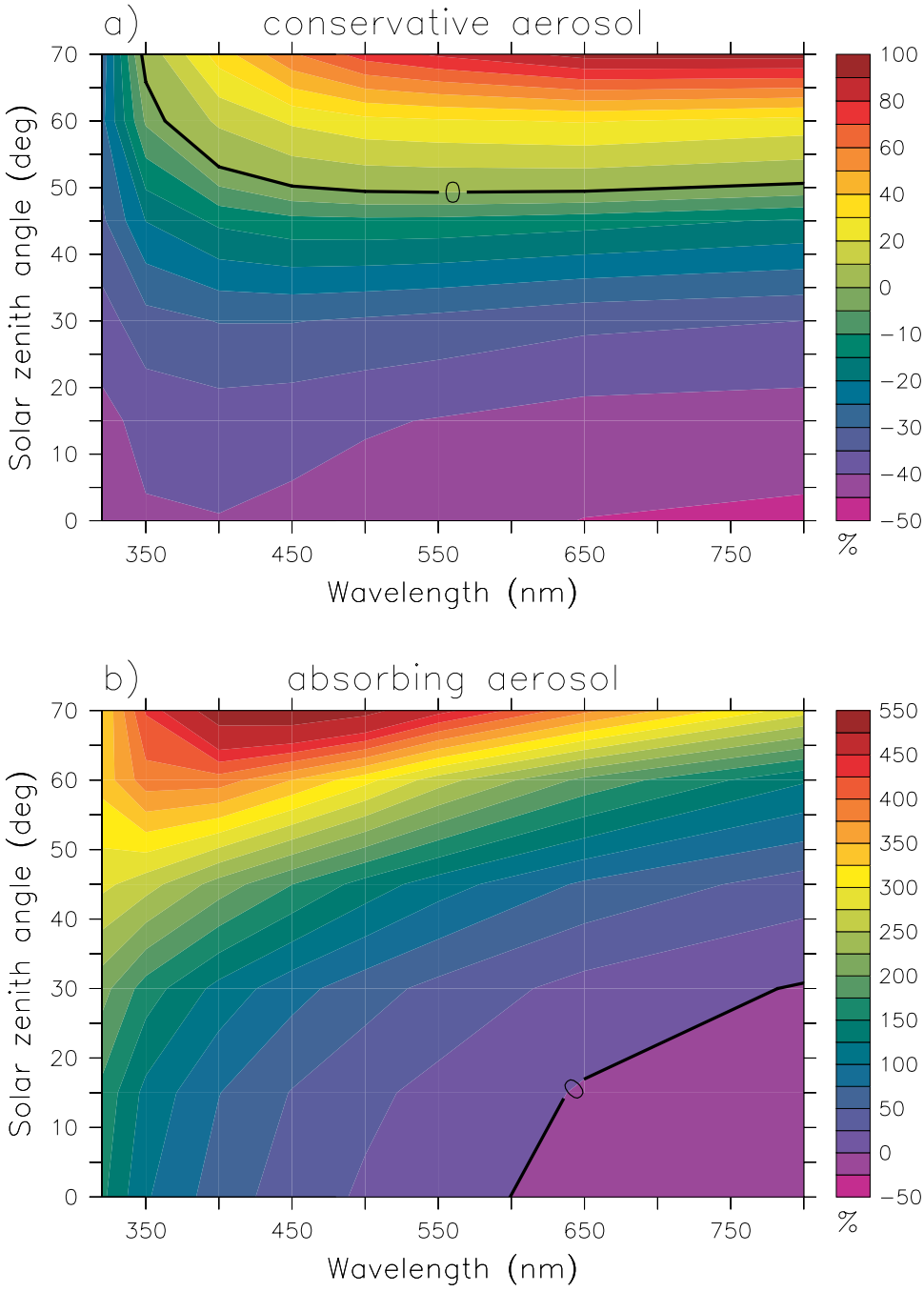

Figure 4. Contour plot of the relative difference of the actinic flux in the plume center between the 3-D and the l-1-D simulation as a function of wavelength and solar zenith angle for the conservative ($\Delta\langle F(1\text{-}1\text{-}D\_CON)\rangle_{pc}$ (REF = 3-D_CON)) (a) and the absorbing ($\Delta\langle F(1\text{-}1\text{-}D\_ABS)\rangle_{pc}$ (REF = 3-D_ABS)) (b) aerosol. For the preparation of these figures, values at a SZA of 15° and at wavelengths of 350, 450, 500, and 650 nm were included in addition to those of Table 2.